

**THE INFLUENCE OF NEAREST-NEIGHBOUR INTERACTIONS AND
ASSEMBLY DYNAMICS ON THE TRANSPORT PROPERTIES OF
PORPHYRIN SUPRAMOLECULAR ASSEMBLIES ON Au(111)**

Alison A. Pawlicki,¹ Ayelet Vilan,² Matthew Jurow,⁴†

Charles M. Drain⁴ and James D. Batteas^{1,3*}

¹Department of Materials Science and Engineering, Texas A&M University, PO Box
3003, College Station, TX 77842

²Department of Chemistry, Weizmann Institute of Science, Herzl St. 234, Rehovot
76100 Israel

³Department of Chemistry, Texas A&M University, PO Box 30012, College Station,
TX 77842

⁴Department of Chemistry and Biochemistry, Hunter College of the City University of
New York, 695 Park Avenue, New York, NY 10021

†Present address: Lawrence Berkeley National Labs, One Cyclotron Road, MS:
67R6110
Bldg. 67, Rm. 6113, Berkeley, CA 94720 USA

≠ Present address: Oak Ridge National Labs and the University of Tennessee,
Knoxville, TN 37830 USA

*Corresponding Author: batteas@chem.tamu.edu

Supporting Information

This document contains details on the Scanning Tunneling Spectroscopy (STS) measurements and the statistical treatment of such measurements. To compare with STS done on ZnTPPF₄-SC₅SH clusters that self-organize on the surface (reported on in the main manuscript), STS was done on pre-formed ZnTPPF₄-SC₅SH clusters and presented herein. In addition, details of Atomic Force Microscopy (AFM) and Scanning Tunneling Microscopy (STM) used to characterize ZnTPPF₄-SC₅SH clusters inserted into a C12 monolayer are discussed. This includes typical microscopy images and monitoring the conductance switching of the ZnTPPF₄-SC₅SH clusters. For all ZnTPPF₄-SC₅SH clusters investigated, we show the apparent height ratio as a function of cluster size and assembly time for the investigated porphyrin clusters.

Method for Scanning Tunneling Spectroscopy (STS) Measurements

A method was developed to measure reliable and repeatable I-V spectroscopy of ZnTPPF₄-SC₅SH within a C12 monolayer. This involves optimization of the STS measurement cycle including the bias intervals. Doing so is paramount because the observation of stochastic switching as discussed in the manuscript depends on the sampling rate and conditioning. Additionally, the STM tip can influence I-V spectroscopy. To minimize this influence thereby obtaining I-V curves characteristic of the ZnTPPF₄-SC₅SH and not of the STM tip, we use a comparison method aided by the analysis of a balance factor which is defined below (Equation S.1).

Scanning Tunneling Spectroscopy (STS) Measurement Cycle

The details of the STS bias intervals are provided in Figure S.1. Each I-V measurement cycle starts with the feedback loop turned on and a 0.1 ms stabilization of the tip above the ZnTPPF₄-SC₅SH or C12 to reach the 20 pA and 1.4 V set-point. Next, the feedback loop is turned off, the voltage is set to the starting point of the measurement (-2 V) and there is an additional 9 ms stabilization before the measurement begins. Then, the bias is scanned from -2 to 2 V for the I-V measurement. After 0.1 ms the feedback loop is tuned on again and allowed another 0.1 ms of stabilization before repeating the cycle. The cycle is repeated 10 times after which the tip is manually repositioned and the spectroscopy is carried out again to obtain a total of 100 curves. Therefore, with the exception of the first spectra in the cycle, there is a 0.2 ms stabilization of the tip using the feedback loop before each measurement. During the measurement, 40.16 ms elapse before the feedback loop is turned on again and the tip height is reestablished above the ZnTPPF₄-SC₅SH or C12 according to the 20 pA and 1.4 V set-points.

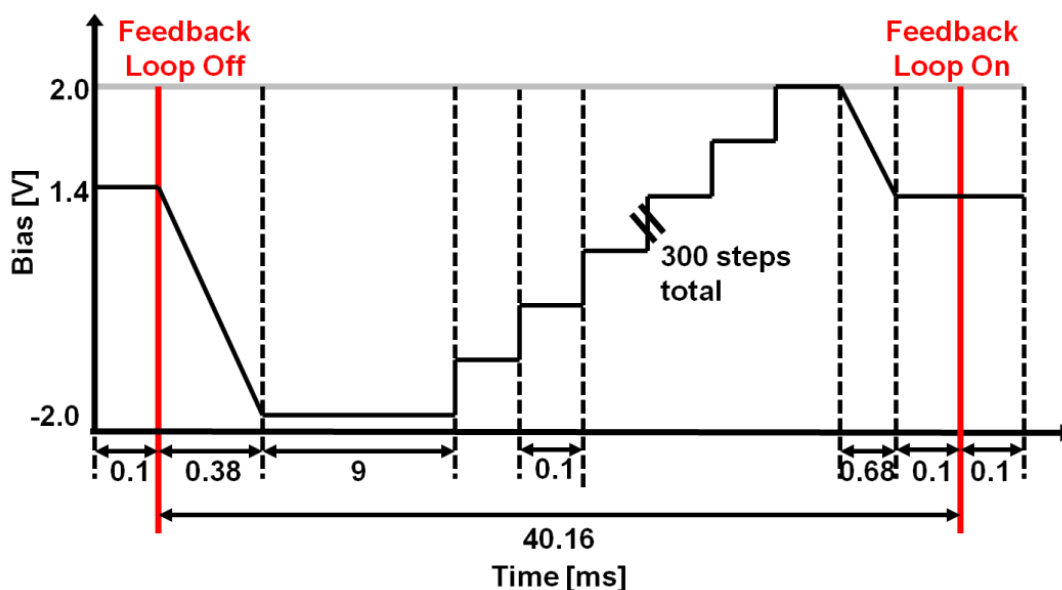


Figure S.1. Schematic diagram displaying one I-V spectroscopy cycle, including delay and acquisition times.

Examining C12 I-V Curves Using a Balance Factor

To minimize spurious tip effects, like tip contamination or degradation, during I-V spectroscopy on ZnTPPF₄-SC₅SH, 100 I-V curves were collected on a near-by C12 matrix area immediately before and after the ZnTPPF₄-SC₅SH spectroscopy. If these reference spectra were of wide distribution or not well behaved, the results were discarded. To examine the distribution and behavior of the C12 I-V curves, a balance factor was used. The balance factor is defined as

$$Balance = \frac{\int_0^2 I(V)^2 V^2 dV - \int_{-2}^0 I(V)^2 V^2 dV}{\int_{-2}^2 I(V)^2 V^2 dV} \quad \text{Equation S.1}$$

where I is the current and V is the voltage. The balance factor was applied to each of the 100 C12 I-V curves and the results were examined in a histogram (Figure S.2). A set of narrowly distributed and well behaved I-V curves is characterized by a balance factor

histogram with a sharp peak in the range of -0.8 to -0.5 (Figure S.2 (A)). If the balance factor histogram does not have a well-defined peak and / or is outside of this range, then the data set is discarded (Figure S.2B)).

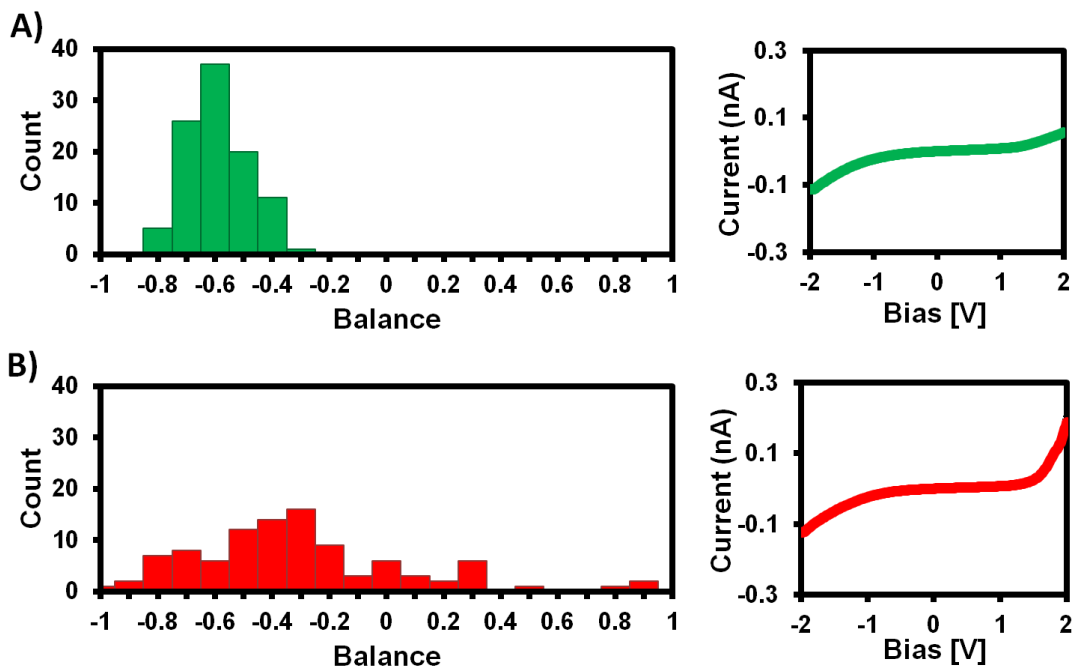


Figure S.2. Representative balance factor histograms obtained from 100 I-V curves of C12 (shown adjacent). In A) the data set is accepted because the histogram has a peak at between -0.8 and -0.5 and is narrowly distributed. However, in B) the data set is discarded because these criteria are not met.

Quantifying Statistics

Statistical treatment of the presented data is described here. These statistics are utilized to quantify the bias-induced switching, observed for the ZnTPPF₄-SC₅SH clusters formed after three days of self-assembly, and stochastic switching, observed in ZnTPPF₄-SC₅SH clusters formed after five days of self-assembly.

Distribution of Geometrical Parameters

The distribution of geometrical parameters, such as the AFM physical height, the estimated molecular tilt derived from the AFM physical height difference, the STM apparent height, and lateral cluster dimension obtained from STM topography, and the apparent height ratio, all show non-symmetric distributions, which could not be fitted to a normal distribution. Table S.1 is an extension of Table 1, providing the major statistical characteristics of the different parameters.

Property	Location	D1	D3	D5	Shape	D1	D3	D5
AFM Phys. Height (nm)	Mean	0.27	0.36	0.36	STD	0.11	0.19	0.17
	Median	0.24	0.30	0.31	IQR / 2	0.04	0.06	0.05
	Mode	0.21	0.26	0.29	Skew	2.42	3.87	6.70
Tilt Angle (degree)	Mean	43.3	41.0	40.5	STD	4.4	4.6	4.3
	Median	44.6	42.6	41.9	IQR / 2	1.5	1.9	1.7
	Mode	45.5	43.5	43.0	Skew	-2.8	-2.3	-3.1
Lateral Dimension (nm)	Mean	6.16	4.13	4.12	STD	4.06	2.57	2.66
	Median	5.23	3.55	3.28	IQR / 2	1.92	1.57	1.70
	Mode	3.20	2.00	1.80	Skew	2.53	1.95	1.54
STM App. Height (nm)	Mean	0.74	1.30	0.64	STD	0.53	0.87	0.48
	Median	0.62	1.04	0.45	IQR / 2	0.26	0.60	0.20
	Mode	0.35	0.50	0.35	Skew	2.56	1.29	2.09
App. Height Ratio (Eq. 2)	Mean	0.54	1.00	0.34				
	Median	0.42	0.74	0.15				
	Mode	0.15	0.24	0.05				

Table S.1. Statistical analysis of the geometric characterization with the parameters as following. Location describes the different ways to extract a characteristic quantity, including the mean defined as arithmetic average over all measured values; median defined as the 50% probability value; mode defined as the highest occurrence value (or highest value of the histogram). The mode was computed on intervals of 0.01, 0.5, 0.1 and 0.05 for AFM height, tilt, lateral dimension and STM height, respectively. Shape describes the different statistical features of the distribution, including STD defined as the standard deviation of the sampling; IQR / 2: defined as half of the interquartile range which is the difference between the 75th and 25th percentiles, and skew is a measure of the distribution asymmetry that equals 0 for a symmetric distribution.

Two of the parameters in Table S.1 are not measured but computed. The estimated tilt angle is extracted from the AFM physical height, compared to nominal ZnTPPF₄-SC₅SH and C12 lengths according to Equation 1 (equation numbers refer to main text). The difference between the AFM physical height (Figure S.3) and STM apparent height (Figure S.4) are used to compute the apparent height ratio (Figure S.5) according to Equation 2. This comparison is that of a population, because STM and AFM were measured by two different instruments on different locations of the sample. The values in Table 1 refer to calculations using the difference between the mean, median, or mode of the STM apparent height and the same characteristic of the distribution in the AFM physical height. The distribution in relative conductivity via the apparent height ratio as presented in Figure S.5 was computed by using individual STM apparent height values subtracted from mean AFM physical height within the same sample. Figure S.5 shows a satisfying correlation between the methods, which strengthens the relevance of the estimated distribution in relative conductance.

Figure S.3 to Figure S.7 displays the histograms of the different parameters and over them the mean, median and mode as vertical lines. These three parameters coincide for normal distribution, which is clearly not the case here. In all cases, the median (“2”, magenta) is the central of the three location values, and therefore, better describe gross shifts in the distribution with time. Therefore, this parameter is chosen to represent the location of the distribution. The mode is generally the least sensitive to the behavioral

evolution with immersion time, suggesting that there is a significant portion of the clusters that do not evolve much with time.

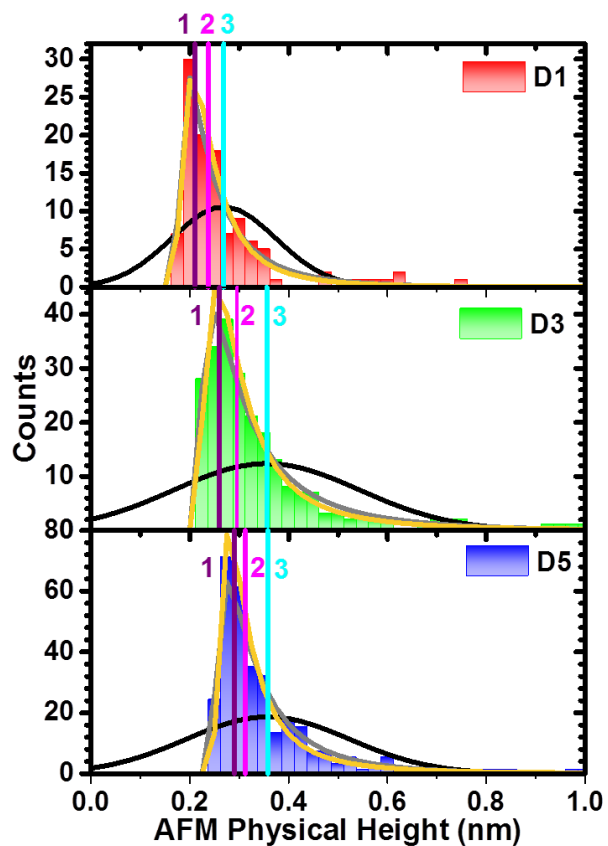


Figure S.3. Distribution of the physical heights measured by AFM. Each panel is for a different immersion time; vertical lines show the mode (1), the median (2) and the mean (3). Curves are fits of the raw data (not histograms) to a Gaussian (black), inverse Gaussian (orange) and generalized extreme value (gray) distribution.

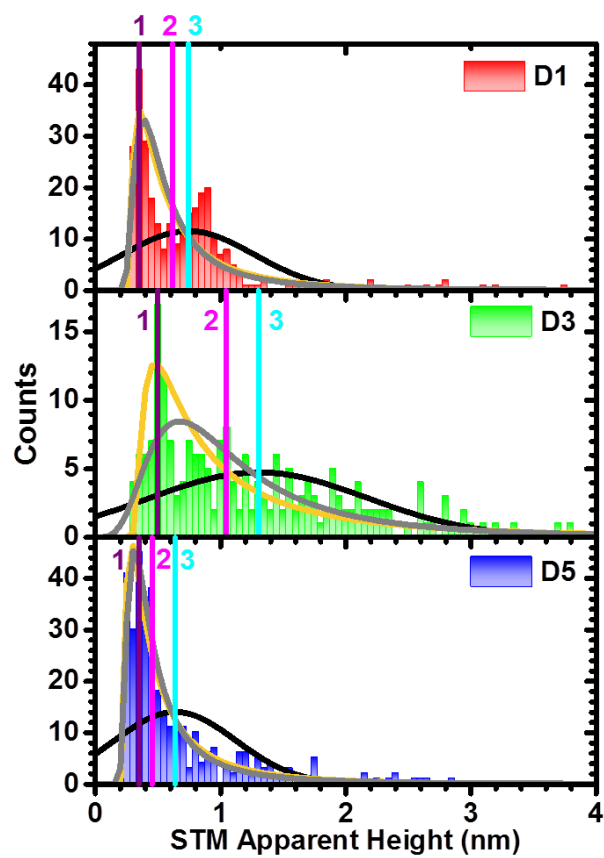


Figure S.4. Distribution of the STM apparent heights. Curves and lines are defined in Figure S.3.

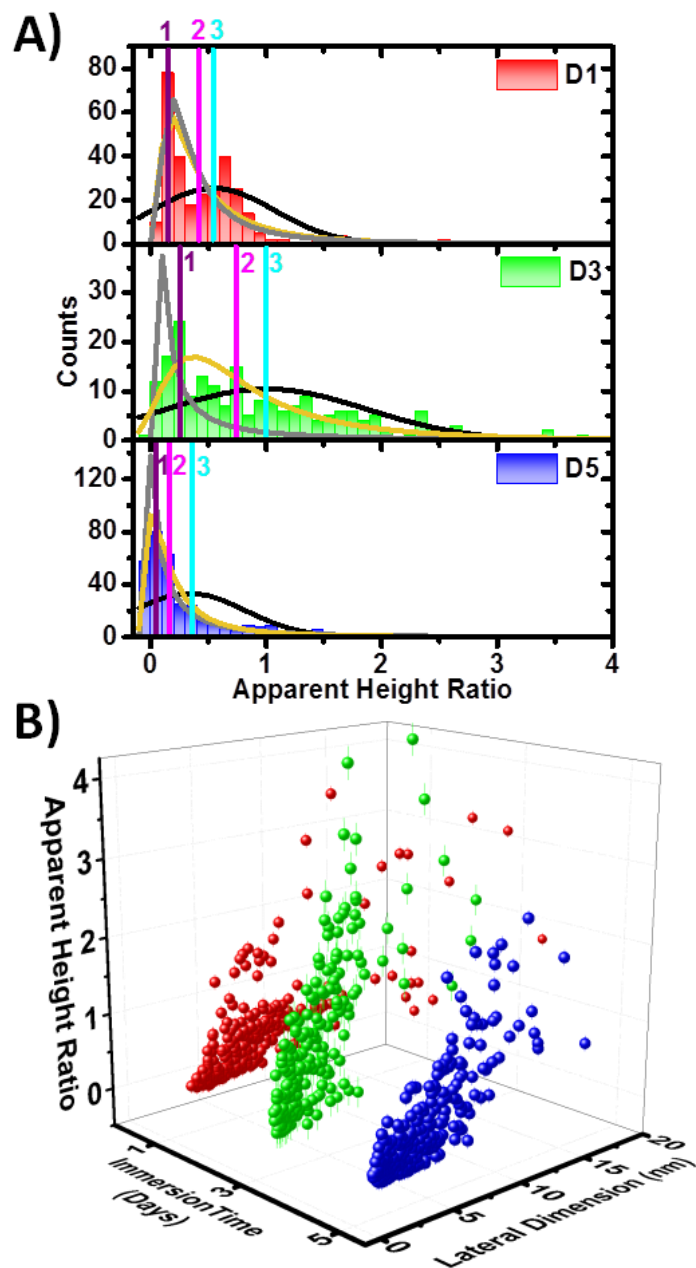


Figure S.5. Distribution of the estimated relative conductivities per Equation 2. A) The apparent height ratio is plotted in histograms. Curves and lines are as above. B) The apparent height ratio is plotted in a three-dimensional plot to display this parameter simultaneously against the lateral cluster dimension and the immersion time. The spread in the apparent height ratio becomes larger as the lateral cluster dimension increases; suggesting that lateral dimension is not the solitary factor impacting the electronic properties.

The different sampling arrays were also fitted to three distribution functions: normal (black curve), inverse Gaussian (orange curve) and generalized extreme value (gray curve). As can be seen in Figure S.3 to Figure S.7, the center of the normal distribution coincides with the mean location (vertical line “3”). The width of the normal distribution or the formal standard deviation is much larger than the real width of the distribution. Therefore, we find the interquartile range (IQR) to be a better representation of the width of the distribution than the standard deviation.

The asymmetry of the data is clearly not in accord with a normal distribution. A common distribution to model nonnegative positively skewed data is inverse Gaussian (orange curves), which gave a fairly good fit to the data. However, we fit the data to this model, only after adjusting the data to start rising at 0 (i.e., fitting used $z = x - \min(x)$ as the independent parameter). Another distribution function that yielded fair description of the data is generalized extreme value (gray curves). This distribution is aimed at describing maximum or minimum values within a random variable; this might reflect the variability in lateral cluster dimensions which has a limited minimum value (equal to a single molecule) and an unbounded upper value.

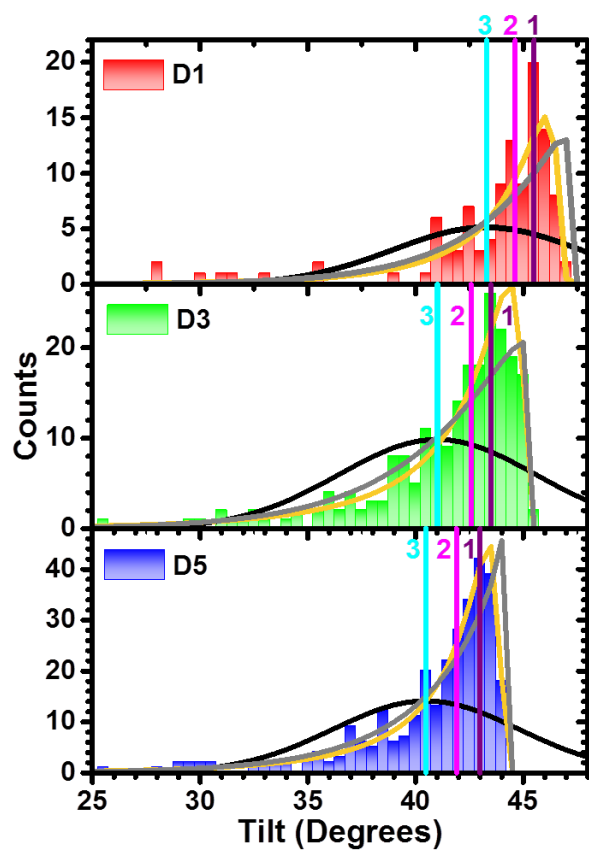


Figure S.6. Distribution of the computed tilt angles (Equation 1) from the AFM physical height. Vertical lines show the 1) mode, 2) median and 3) mean. The curves are fit to a Gaussian (black), inverse Gaussian (orange), and generalized extreme value (gray) distribution. Note that the negatively skewed data was fitted to an inverse Gaussian by using $z = x - \min(x)$.

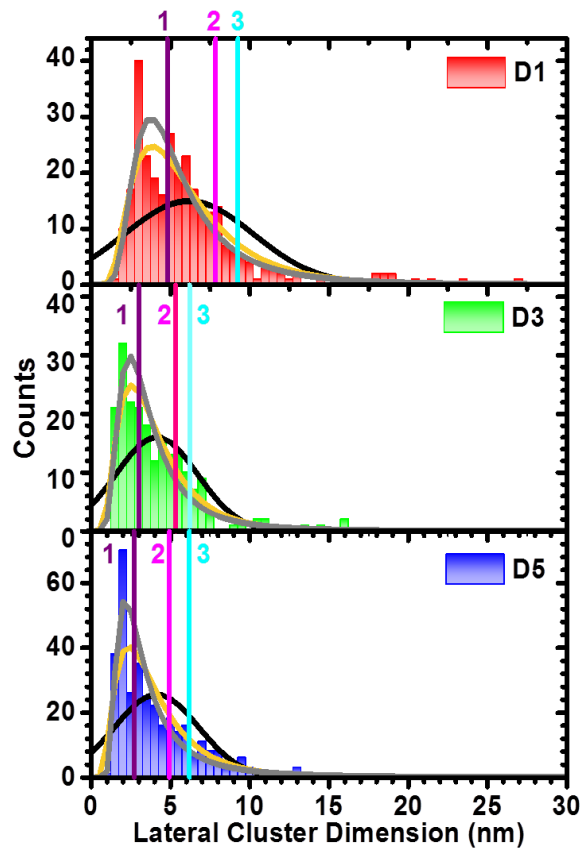


Figure S.7. Distribution of the lateral cluster dimension as extracted from STM images. Curves and lines are as above.

Quantifying Bias-Induced Switching by Defining the Noise Level

The noise level is set to a value of 0.5 pA based on the observed noise in measured current (i.e. 2.5% of the set-point current and 0.02% of the amplifier saturation). Figure S.8(A) illustrates the extraction of V_{noise} on an arbitrary I-V trace (trace D3 of Figure 4 of main text). All data within noise level are colored red. Between ca. 0.5V to 1V data are fluctuating below and above the noise threshold, which makes it difficult to define a sharp voltage edge. The solution was to simply count all data within this threshold (the

number of red points in Figure S.X(A), and then multiply them by the bias interval ($\delta V = 13.3 \text{ mV}$) to translate the counts in voltage scale:

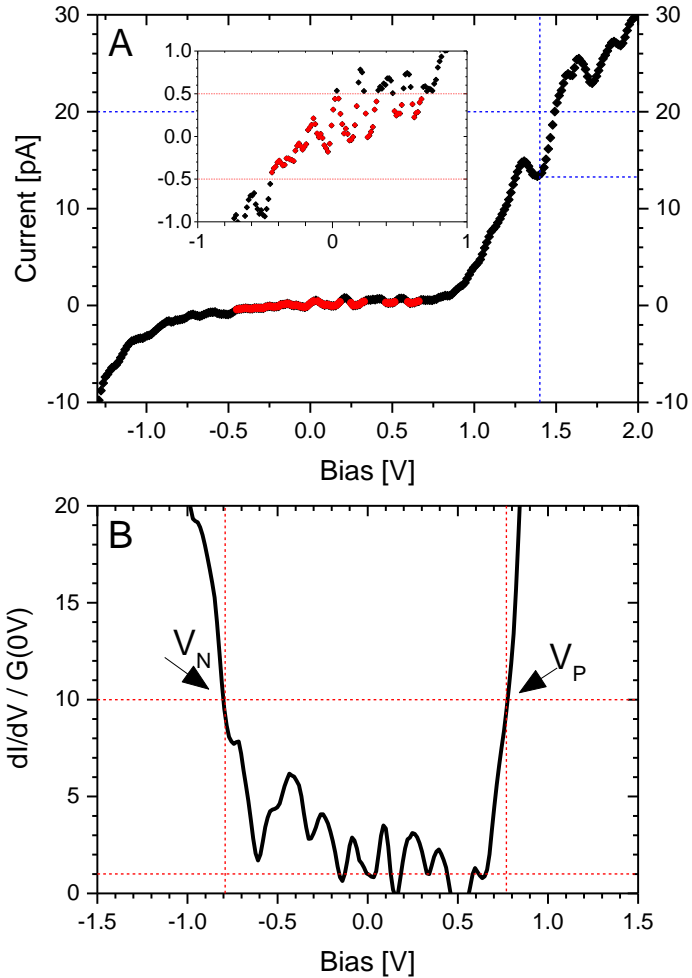


Figure S.8. Demonstration of extracting the characteristic parameters, showing A) noise window, V_{noise} and set-point ratio, P_{sp} , and B) tunneling window, V_{tunn} . The inset to (A) is a zoom-in over the $\pm 1\text{V}$ range, where the two horizontal red line depict the noise threshold of 0.5 pA. All data within this range are colored red. The blue lines in (A) depict the set-point voltage (1.4 V vertical line) and set point current (20 pA, top horizontal line) and the actual measured value (bottom line). The P_{sp} ratio in this case is 13/20. Panel (B) illustrates the extraction of V_{tunn} by plotting the numerically derived dI/dV divided by its value at 0V, forcing $Y=1$ at $X=0$ (bottom horizontal line). The arbitrary threshold of 10 folds is depicted by the upper horizontal line, and the two vertical lines mark where the experimental trace crosses this threshold.

$$V_{noise} = \delta V \cdot [\sum_{all V} (|I| < 5 \cdot 10^{-13}) - 1] \quad (\text{Equation S.2})$$

where the square brackets term is the sum of intervals. Equation S.2 is approximated because it does not differentiate between a continuous low state and stochastic turn-offs. For example, the inset to Figure S.8(A) shows that in this case, the actual fluctuating (noise) region is larger than the number of red dots (prediction of Equation S.2).

Definition of Tunneling Window

The conductance gap is very clear on a derivative plot as shown in Figure S.8(B), showing the same raw data as in Figure S.8(A) after numerical differentiation (using 20-points smoothing). The Y-axis is scaled according to the conductance value at 0V, such that the upper red line depicts the 10 folds threshold. The so-called tunneling region stretches from V_N , the bias voltage where the trace crosses the threshold on negative bias to V_P , the positive voltage of crossing: $V_{P(N)}$ = lowest (highest) bias where

$$\frac{dI}{dV} \geq 10 \cdot G_{Eq} \quad (\text{Equation S.3})$$

$$V_{tunn} = V_P - V_N \quad (\text{Equation S.4})$$

Distribution of Equilibrium Conductance

The conductance of STM measurements is always relative to the set point. Therefore, the 0 V (equilibrium) conductance is basically a measure of the dynamic range of the junction (the conductance at the set-point is fixed to $20\text{pA} / 1.4 \text{ V} = 1.4\text{E-11}$).

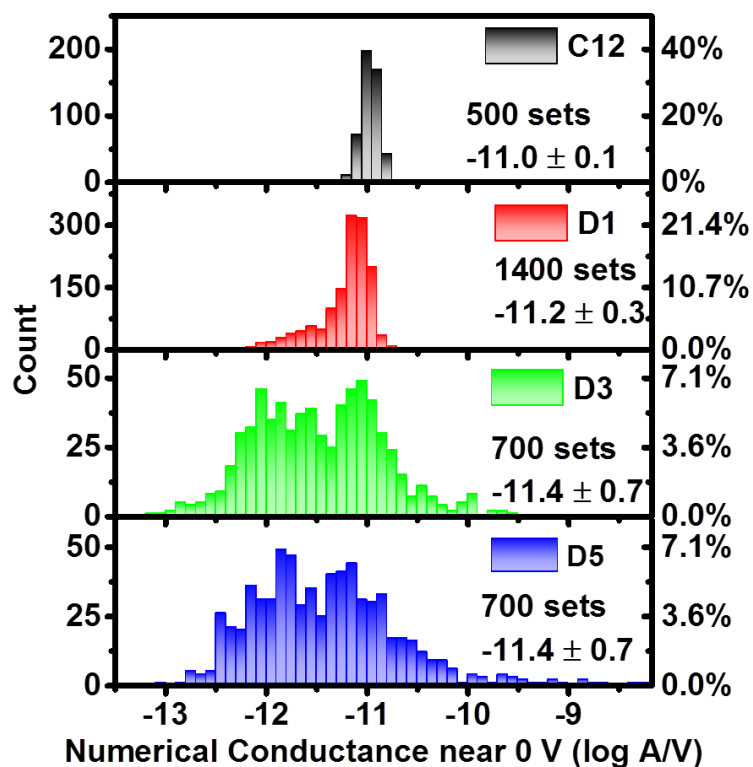


Figure S.9. Histograms of the equilibrium conductance (G_{Eq}) for all measured data. The equilibrium conductance is derived by averaging the four data points between ± 20 mV of the numerically extracted conductance. The G_{Eq} values shown here are the reference values used to compute the low-conductance gap (V_{tunn}).

Figure S.9 shows the equilibrium conductance of C12 is only slightly below the set point value (ca. $1E-11$ cf. $1.4E-11$). In contrast the D3 and D5 clusters show a marked shift of the equilibrium conductance to 1 - 2 orders of magnitude lower values, due to bias-switching (the set-point occurs in an “on” state). In addition, stochastic fluctuations also yield conductance values above the set point.

Lack of Time Dependence in Stochastic Switching

The extraction of set-point ratio (P_{sp}) is demonstrated by the blue lines in Figure S.8(A).

In this specific case, P_{sp} is rather low ($13/20 = 0.65$).

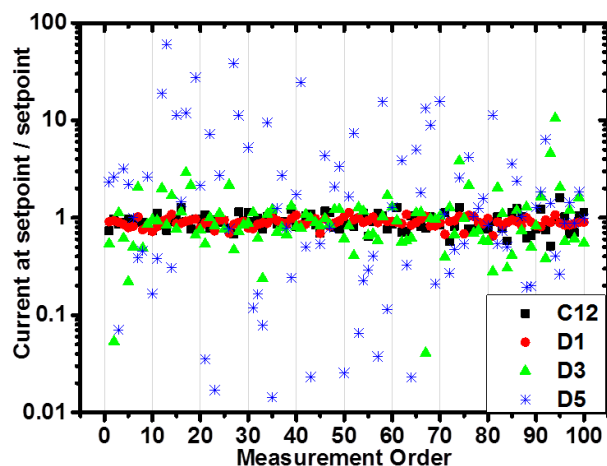


Figure S.10. Stability of set-point current with successive scans, showing the set-point current ratio, P_{sp} (see Equation 3 of main text) for 100 successive scans at a constant tip location versus their recoding order. Each symbol refers to different immersion times. The data set is identical to the one used in Figure 3.

Spectroscopy of Pre-Formed ZnTPPF₄-SC₅SH Clusters

In order to gain support for the pi-stacking explanation, it was attempted to induce stronger aggregation by increasing the concentration of ZnTPPF₄-SC₅SH in the immersion solution from 0.05 mM to 0.5 mM. The 10× higher concentration yielded over-crowding of ZnTPPF₄-SC₅SH clusters, and physical deposition (molecular clusters which are weakly-bound to the substrate and easily adsorbed onto the STM tip). About 30% of the ZnTPPF₄-SC₅SH clusters formed after one day in high-concentration

ZnTPPF₄-SC₅SH showed I-V behavior similar to that of aged clusters formed after three days in the low-concentration ZnTPPF₄-SC₅SH solution (Figure S.11 in the Supporting Information). The fact that increased solution concentration induces behavior similar to that achieved by slow surface cluster growth, suggests that the driving force for this process originates in molecular interactions rather than other mechanisms such as rearrangement of surface adatoms, which should not be affected by the solution concentration.

Immersing the C12 matrix in high concentration (0.5 mM cf. 0.05 mM reported in the main manuscript) of ZnTPPF₄-SC₅SH solution for only one day yielded a highly-crowded mixed monolayer. These samples were difficult to characterize by STM because substance appeared to be deposited on the tip. Still, it is assumed that the high concentration and high deposition rate enhanced the aggregation within the clusters and therefore serves as important evidence for the effect of local organization on transport. AFM characterization of the high-concentration clusters yielded practically identical physical height to that of clusters made by immersion in low-concentration. STM, in contrast, indicated distinctly different behavior of ZnTPPF₄-SC₅SH clusters made after immersion for one day in high- compared to low-concentration solutions. While immersion in low-concentration yielded fairly reproducible clusters and STS curves after one day, immersion in a high-concentration solution for the same duration yielded a large height distribution and marked differences in the I-V behavior varying from continuous tunneling to a pronounced gap-opening, as observed for longer immersion times in a low-concentration solution. A total of 14 clusters were characterized by STS,

with 100 repeating scans on each cluster. Six of the clusters had an STM apparent height of 2.5 to 4 nm cf. apparent height ≤ 1.5 nm for low-concentration D1 samples. The rest of the tested clusters were divided to two sub-groups of four in each, showing I-V behavior similar to either short immersion (D1) in low-concentration or long-immersion time (D3) in low concentration. I-V parameters for these two sub-populations are shown as bar histograms in Figure S.10. For comparison, the distribution of I-V parameters measured over low-concentration clusters are over-plotted as lines for one day (“D1”, red) and three days (“D3”, green).

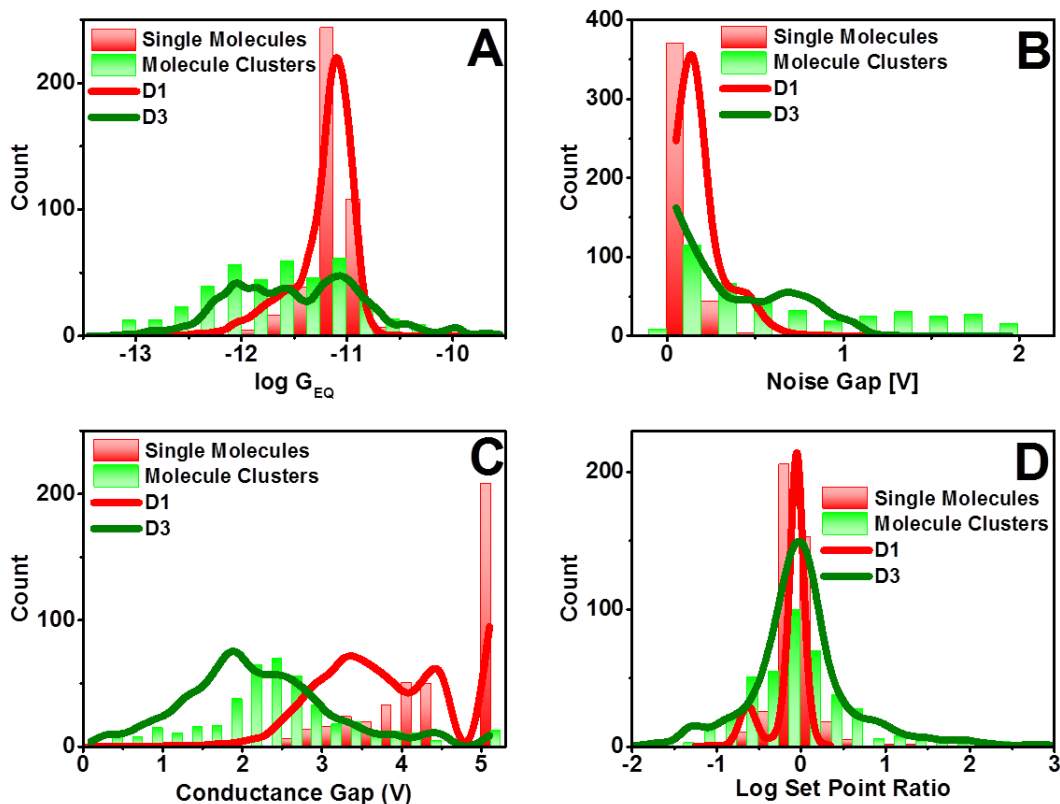


Figure S.11. Histograms of I-V parameters of ZnTPPF₄-SC₅SH clusters formed after one day immersion in 0.5 mM solution (10 times the normal concentration). Bars are histograms of single molecules and molecular clusters; Curves are references showing histogram values for clusters made by immersion time in low-concentration solution for

one day (red) and three days (green). Each panel shows a different parameter: A) Conductance near 0 V (see Figure S.10), B) the noise bias gap (see Figure 5(A) and Equation S.2), C) the low-conductance bias gap (Figure 5(B), Equations S.3,S.4), and D) the set-point log-ratio (Figure 6 and Equation 3 of the main text).

Microscopy Images of ZnTPPF₄-SC₅SH in C12 Monolayer

ZnTPPF₄-SC₅SH clusters were characterized by Atomic Force Microscopy (AFM) and Scanning Tunneling Microscopy (STM). Typical AFM and STM topography images (on different locations) are shown in Figure S.12 and Figure S.13. The height of the clusters measured from either AFM or STM is the difference with respect to the C12 monolayer. The height measured from AFM is the physical height, δ_{AFM} , and from STM is the apparent height, δ_{STM} . Additionally, the lateral dimensions of the clusters are extracted from STM images due to finer lateral resolution than AFM. As an example of this height and lateral dimension measurement, cross sections of ZnTPPF₄-SC₅SH clusters are shown in Figure S.12(C) and Figure S.13(C).

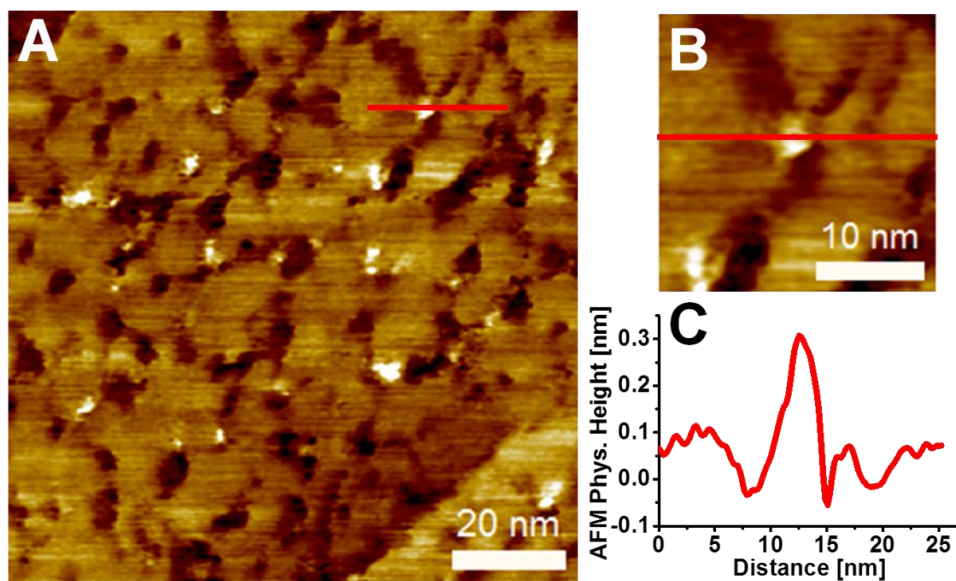


Figure S.12. Typical AFM topography of ZnTPPF₄-SC₅SH clusters in the C12 matrix. A) AFM topography image where the white features are ZnTPPF₄-SC₅SH clusters. B) A closer look at a certain ZnTPPF₄-SC₅SH cluster from the image shown in A). A cross section is taken from this ZnTPPF₄-SC₅SH cluster and the profile is shown in C). The difference between the background C12 and the maximum height of the ZnTPPF₄-SC₅SH cluster is the physical height.

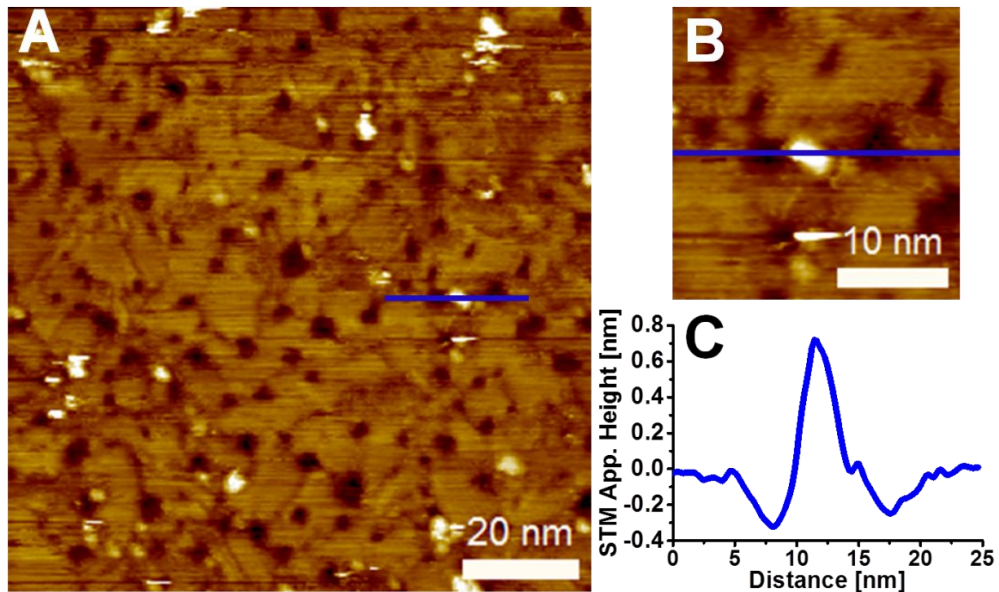


Figure S.13. Typical STM topography of ZnTPPF₄-SC₅SH clusters in the C12 SAM. A) STM topography image where the white features are the ZnTPPF₄-SC₅SH clusters. B) A closer look at a certain ZnTPPF₄-SC₅SH cluster from the image shown in A). A cross section is taken from this ZnTPPF₄-SC₅SH cluster and the profile is shown in C). The difference between the background C12 and the maximum height of the cluster is the apparent height. Although this is not the identical cluster shown in Figure S.13, in general the apparent height is larger than that of the physical height. The larger apparent height is due to the increased conductivity of the ZnTPPF₄-SC₅SH clusters with respect to the C12 SAM.

Stochastic Switching as a Function of STM Imaging Time and Set-Point

The conductive state of ZnTPPF₄-SC₅SH clusters formed after five days were examined by repeated and continuous STM imaging with constant imaging set-points at 1.4 V and 20 pA. Figure S.14 displays the STM images recorded during 15 cycles. Initially there are 14 ZnTPPF₄-SC₅SH features visible as bright protrusions in the defined scan area. The apparent height and lateral dimensions of the visible ZnTPPF₄-SC₅SH features were monitored throughout the 15 cycles. Three of these features are shown below where one

ZnTPPF₄-SC₅SH feature is displayed in Figure S.13(D) and the data presented in Table S.2 and two ZnTPPF₄-SC₅SH features are displayed in Figure S.14(C) and the data presented in Table S.3. The apparent height of these three features stochastically fluctuates from a large apparent height, as large as 2.8 nm, to a small apparent height, as small as 0.3 nm. Additionally, in some cases, the ZnTPPF₄-SC₅SH feature disappears and is no longer apparent in the STM image, then reappears in a later image cycle (Figure S.14(C) and Table S.3). Fluctuations in the apparent height indicate that the conductive state of these ZnTPPF₄-SC₅SH clusters is dynamic under these imaging conditions. ZnTPPF₄-SC₅SH clusters stochastically fluctuate from a highly conductive “on” state (large apparent height) to a low conductive state (small apparent height) and to an even lower “off” conductive state (non-existent apparent height). In the final image, only one of the ZnTPPF₄-SC₅SH clusters was still visible in the “on” state while the others switched to the “off” state (Figure S.14(B)). When the image range was expanded to include the previously un-imaged surrounding area, it was clear that only the continuously imaged area was devoid of apparent ZnTPPF₄-SC₅SH features as evidenced in Figure S.14(A-C). For prolonged imaging beyond the 15 cycles described here, the ZnTPPF₄-SC₅SH features seldom re-appeared. This suggests that prolonged STM imaging under 1.4 V and 20 pA eventually turns “off” the ZnTPPF₄-SC₅SH clusters in which the conductance state settles into a possible local potential minimum. Therefore, stochastic conductance switching was observed by repeated and continuous STM imaging at 1.4 V and 20 pA but eventually stochastic switching is overruled by switching “off” due to prolonged imaging.

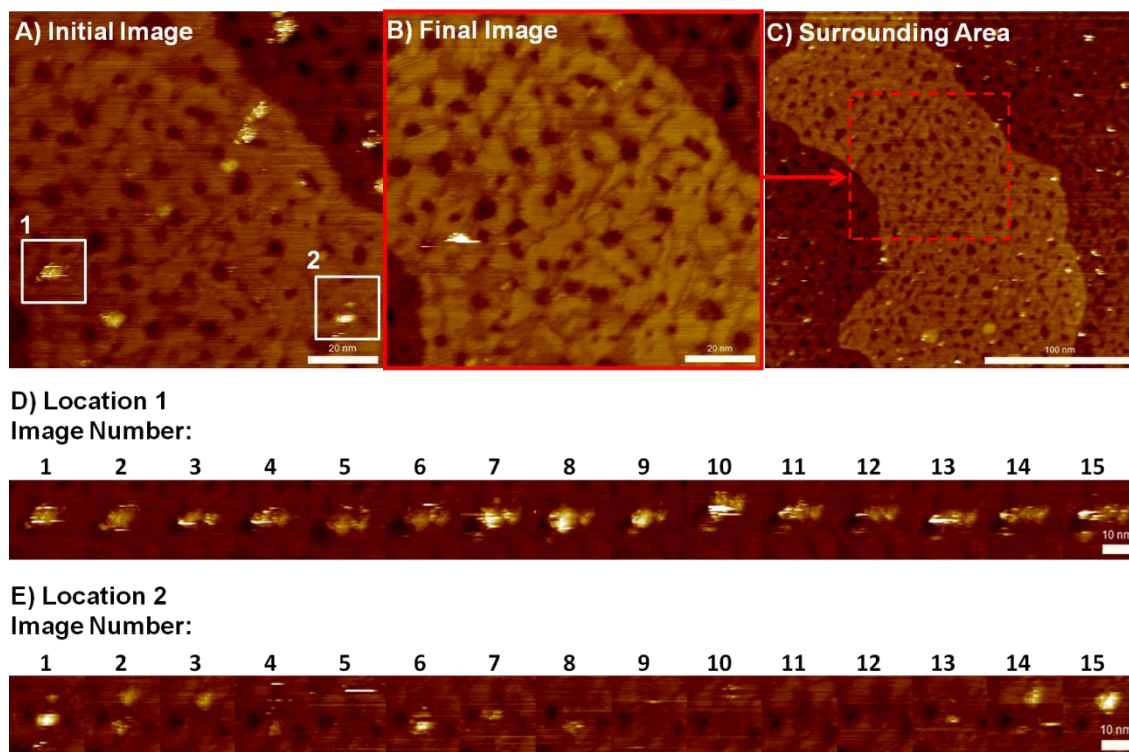


Figure S.14. Investigation of stochastic switching in ZnTPPF₄-SC₅SH clusters formed after five days by repeated and continuous STM imaging maintaining constant imaging set-points; 1.4 V and 20 pA. A) The initial STM image recorded in the series in which 14 ZnTPPF₄-SC₅SH features are visible. The scale bar is 20 nm. B) The final STM image after 15 continuous images in which only 1 ZnTPPF₄-SC₅SH features is visible. The scale bar is 20 nm. C) After the final image was recorded, the scan range was expanded to include the surrounding area. It appears that there are ZnTPPF₄-SC₅SH features only in the surrounding, previously un-scanned area. The scale bar is 100 nm. Repeated and continuous STM images of a particular ZnTPPF₄-SC₅SH feature at D) location 1 and E) location 2 as indicated in A). The scale bar is 10 nm.

Location 1															
Image Number	1	2	3	4	5	6	7	8	9	10	11	12	13	14	15
Apparent Height (nm)	1.6	0.7	2.1	2.2	0.9	0.9	1.8	1.5	1.4	2.8	1.7	1.5	2.8	1.3	2.2
Lateral Dimension (nm)	11.8	11.3	8.3	12.5	12.2	8.9	18.1	10.6	11.5	12.7	15.1	13.9	16.2	16.5	18.1

Table S.3. The apparent height and lateral dimension of the ZnTPPF₄-SC₅SH clusters shown at location 1 in Figure S.14(D) during continuous STM imaging at constant imaging set-points, 1.4 V and 20 pA. The image numbers here are associated with the image numbers in Figure S.14(D). The apparent height stochastically fluctuates from a large apparent height or a highly conductive state to a reduced apparent height or a less conductive state. With the apparent height fluctuations, the lateral dimension fluctuates as well.

Location 2															
Image Number	1	2	3	4	5	6	7	8	9	10	11	12	13	14	15
Apparent Height (nm)	0.4	0.5	0.5	0.5	N/A	N/A	N/A	0.5	0.5	N/A	N/A	N/A	N/A	0.7	0.9
	0.8	0.5	N/A	0.4	0.8	0.5	0.7	N/A	N/A	N/A	N/A	N/A	0.6	0.3	N/A
Lateral Dimension (nm)	3.5	6.4	7.0	1.9	N/A	N/A	N/A	5.4	3.9	N/A	N/A	N/A	N/A	8.3	9.8
	7.9	5.1	N/A	2.7	8.2	6.3	7.1	N/A	N/A	N/A	N/A	N/A	4.1	2.4	N/A

Table S.4. The apparent height and lateral dimension of the ZnTPPF₄-SC₅SH clusters shown at location 2 in Figure S.14(E) during continuous STM imaging at constant imaging set-points, 1.4 V and 20 pA. There are two ZnTPPF₄-SC₅SH features that appear in Figure S.14(E) and both are tracked here in which the uppermost feature is recorded in the upper rows and the bottommost feature is recorded in the gray-highlighted, lower rows. The image numbers here are associated with the image numbers in Figure S.14(E). The apparent height stochastically fluctuates from a large apparent height to a reduced or even a non-existent apparent height (denoted N/A). With the apparent height fluctuations, the lateral dimension fluctuates as well and sometimes is even not apparent (denoted N/A).